RSC Advances

ROYAL SOCIETY OF CHEMISTRY

www.rsc.org/advances

Journal Name

RSCPublishing

ARTICLE

Effects of Atomic Ag on Photocatalyst AgBr surfaces: A Theoretical Survey

Cite this: DOI: 10.1039/xoxxoooooox

Yuhua Chi,[a b] Lianming Zhao,[a b] Xiaoqing Lu,[a b] Wenyue Guo,[*a b] Yunqi Liu,[** c] and Chi-Man Lawrence Wu[d]

Received ooth XX 2014,
Accepted ooth XX 2014

DOI: 10.1039/xoxxoooooox

www.rsc.org/

The electronic states and optical properties of atomic Ag on photocatalyst AgBr surfaces have been investigated using density functional theory plus Hubbard U contributions. Upon the adsorption of Ag on the AgBr surfaces, the adsorbed (110) surface favors a new visible absorption, while a new infrared absorption is largely enhanced for the adsorbed (100) surface. These changes of absorption spectrum are mainly attributed to the MIGS (metal induced gap states) formed in the energy-gap region of the silver bromide. Moreover, the Ag_{ad} wave functions mixing with the orbitals of the silver ions of the silver bromide obviously impact on the energy levels of the conduction band bottom. Photoexcitations of the adsorbed (110) surface involve dominantly electron transfers from Br to the MIGS and the hybridized orbitals in the whole light absorption region, while the new infrared absorption (> 600 nm) is attributed to excitation of states of the Ag_{ad} and the hybridized orbitals on the adsorbed (100) facet. Consequently, the Ag_{ad} can effectively reduce the silver bromide photolysis, so as to enhance its stability. Free-energy profiles of water dissociation on these surfaces also indicate that the Ag_{ad} can effectively improve the photocatalytic activity of silver bromide.

1. Introduction

Semiconductor photocatalysts have attracted wide attention due to their potential applications in the renewable energy and environmental fields.[1-12] Since the photocatalytic reaction occurring on surfaces of semiconductor materials involves a series of catalytic processes driven by solar light, exploring photocatalysts that utilize the solar light irradiation efficiently and possess excellent catalytic performance is essential for their practical applications.[1] In this respect, many efforts have been made to explore specific facet dominated structures of semiconductors and metal-particles adsorbed on photocatalysts.[2-4] Owing to the particular arrangement of surface atoms and unsaturated dangling bonds, the exposed crystal facets play a critical role in determining photocatalytic activity, and nano- or micro-crystalline semiconductors with high-reactivity surfaces usually exhibit high photocatalytic activities. Adsorption of metal particles on facets of semiconductors can also improve the photocatalytic performance.[5-10] Rodríguez et al. found that Cu nanoparticles deposited on TiO_2(110) decreased the apparent activation energy for water-gas shift (WGS) by strong interactions between Cu and titania, favoring high catalytic activity.[11] Plasmonic photocatalysis was enabled by depositing TiO_2 on a nanoparticle (NP) consisting of a silver core covered with a silica (SiO_2) shell to prevent Ag oxidation by direct contact with TiO_2, and this plasmonic photocatalyst exhibited enhanced catalytic activity under UV illumination.[12] However, the main drawbacks of TiO_2 are its low quantum yield and lack of visible light utilization because of the large band gap (3.23 eV of anatase TiO_2). Therefore, it is of great interest to develop universal photocatalysts that efficiently utilize the visible part of the solar irradiation.

Recently, silver halides have become a hot topic in photocatalysis because of their strong visible light absorption and photosensitive characteristics.[13-17] One of the most representatives is the silver bromide, AgBr, with the rock-salt (space group Pm3m) structure crystallized under normal conditions, is a conventional photographic material with a narrow band gap of 2.6 eV. This material exhibits excellent photocatalytic performance under visible-light irradiation, but is seldom used as photocatalyst due to its instability under sunlight. Fortunately, Kakuta et al. found that AgBr decomposition to Ag occurred in the early stages of UV illumination, but covered with Ag clusters it was stable under successive UV illumination.[18] Inspired by this finding, recently, wide attention has been paid to this material, and the properties and activities of various structures of the material have been explored.[19-28] An et al. synthesized AgBr/Ag nanoplates by the precipitation reaction between $AgNO_3$ and NaBr in glycerol with the assistance of polyvinylpyrrolidone (PVP), and found that the as-prepared AgBr/Ag nanoplates exhibit stronger absorption in the visible region than pristine AgBr, due to the contribution of surface silver nanoparticles, enhancing the photocatalytic activity not only towards decomposition of organic pollutants but also towards conversion of CO_2 to methanol under visible light irradiation.[19] Kuai et al. prepared Ag/AgBr by a facile hydrothermal and subsequently sun-light-induced formation method, and found that the as-prepared

AgBr covered with Ag clusters had a strong absorption in the visible region, which was almost as strong as that in the UV region due to the plasmon resonance of the silver nanoparticles deposited on AgBr. This material was stable due to the fact that photons are only absorbed by the silver nanoparticles and electrons separated by absorbed photons remain in the nanoparticles rather than being transferred to the Ag^+ ions of the AgBr lattice.[20] Wang et al. found that Ag nanoparticles deposited on AgBr surfaces could enhance the photocatalytic activity and stability, and that the as-prepared AgBr nanocrystals exhibited interesting facet-dependent photocatalytic properties. For instance, the completely {111} exposed AgBr showed high photocatalytic activities, with the photodegradation rate of methyl orange (MO) dye molecules four times faster than over AgBr with only {100} facets exposed.[21] Zhou et al. studied the degradation of toxic with Ag-$AgBr/Al_2O_3$ under visible-light irradiation, and found that the catalyst shows high and stable photocatalytic activity, and the photocatalysis involves two plasmon-induced electron-transfer processes, i.e., from the excited Ag particles to AgBr and from the organic pollutants to the Ag particles.[23] The coupling of AgBr and Ag provides a distinctive pathway for the discharge of electrons at the electrolyte interface. From the earlier studies, two modes of electron transfer in silver/silver halides were found, i.e., the photoinduced electrons remaining in the silver particles rather than being transferred to silver halides,[19-22] and the photoinduced holes remaining on the silver particles.[23, 24]

On the theoretical side, Baetzold investigated small silver clusters containing 1-5 atoms adsorbed to kink sites or flat regions that exist on the AgBr(001) surface using density functional calculations. His results suggest that the positive kink site is unique in providing a location where the neutral cluster can capture photoelectrons, other kink sites with neutral or partial negative charges act only as locations for chemically-produced silver clusters, which do not permit electrons trapping at neutral silver clusters.[25,26] Rabilloud studied the structural and electronic properties of Ag_nBr_p(n<6, p=n-1) clusters, the results indicated that all external electron of the metallic site are mainly transferred to the halogens except that of the extra silver atoms.[27] Wang et al. studied AgBr-based photocatalysts using the periodic slab model, and found that the {111} facets have higher surface energy and thus are more reactive than the {100} facets, which agrees well with the experimental result.[21] However, theoretical studies of the effect of the silver clusters on AgBr surface properties are very few, which is very important for the understanding of the photocatalytic mechanism of silver/silver bromide. In this work, the interaction of silver with different surfaces and the effect of Ag on the surface photocatalytic properties are studied, based on density functional theory (DFT) incorporating the LDA+U formalism using an embedded cluster model. It is well known that first-principles DFT severely underestimates the band gap of semiconductors, an on-site Coulomb repulsion parameter, i.e., the Hubbard parameter (U), is employed to incorporate part of the electron correlations absent in DFT.[29, 30] With the on-site electron correction, both the band gaps and the location of additional states introduced by adsorbed metal atom can be properly described. The thermodynamically stable (100) and (110) facets of AgBr are selected as the representative of this work to study the facet-dependent effects of the photocatalyst. The atomic Ag adsorption on both facets is employed as an approximate model of the metal-surface system, according to experimental characterization of catalysts[13, 20] and the concept of single-atom heterogeneous catalysis.[3] The geometric structures, electronic structures, and optical properties of the clean and adsorbed facets are investigated in detail, and the catalytic activities of these facets are investigated by using water dissociation as a benchmark probe reaction. The theoretical results are compared with the experimental findings and could provide a theoretical guidance to the photocatalytic experiments.

2. Methods and Computational Details

All calculations are spin-polarized and carried out using DFT incorporating the LDA+U formalism implemented in the CASTEP code[10] and employing norm-conserving pseudopotentials. The geometric structures were optimized using the generalized-gradient approximation (GGA)[31] and the exchange-correlation functional of Perdew-Burke-Ernzerhof (PBE)[32] correlation functional prior to performing the LDA+U calculations.[33] The valence configurations were $4d^{10}5s^1$ for Ag and $4s^24p^5$ for Br. The parameters setting for the calculations were as follows: the force on atoms was less than 0.03 eV/Å, the stress on atoms was less than 0.05 GPa, the atomic displacement was less than 0.001 Å, the energy change per atom was less than 1×10^{-5} eV, and the kinetic energy cutoff was 500 eV. In the cases of surface slabs, a vacuum region of 15 Å was chosen to eliminate the influence from the adjacent bottom layer. For each surface, stoichiometric slab models were used, which consisted of six atomic layers. The bottom four layers were fixed to their bulk positions, while the other two were allowed to relax. The Monkhorst-pack sets of k points used for the Brillouin zone sampling were different depending on the supercell dimensions, and were set as 3×3×3 for bulk AgBr, 2×2×1 for (2×2) surface slabs, and 3×3×1 for (3×3) surface slabs. Extensive test calculations were performed to determine the appropriate U parameters for Ag(d) and Br(p) that reproduced correctly the electronic band gap and the location of electron states for bulk AgBr. The U values thus obtained were $U_{d,Ag}$=1.6 eV, $U_{p,Br}$=1.3 eV (see Table S1 in the Electronic Supplementary Information (ESI)).

The cohesive energy E_{coh} was computed by using the following formula:

$$E_{coh} = \frac{E_{sup} - nE_{Ag} - nE_{Br}}{n}$$

where E_{sup} is the total energy of the super cell, E_{Ag} and E_{Br} are energy of the single Ag and Br atom, respectively, n is the number of atoms contained in the super cell.

Based on the geometry relaxations, the surface energy (γ) was computed using the following formula:[32]

$$\gamma = \frac{E_{slab} - nE_{bulk} - N_X E_X}{2A}$$

where E_{slab} is the total energy of the slab, E_{bulk} is the total energy of the bulk per unit cell, n is the number of bulk unit cells contained in the slab, N_X is the number of adsorbed X atom, E_X is the energy of the adsorbed X atom and A is the exposed area of one side of the slab.

The curvature of the parabolic portions of bands near the conduction-band minimum (CBM) and valence-band maximum (VBM) was studied. The following simple relation equates the curvature of the bands to the effective mass of electrons or holes:[29]

$$m^* = \frac{\hbar^2}{2\alpha}$$

where m^* is the effective mass of the charge carriers, $\hbar$ is the Plank constant, and α is the coefficient of the second order term in a quadratic fit of $E(\boldsymbol{k})$.

The details of the Gibbs free-energy calculations of water splitting on surfaces have been presented in reference [34]. In

the reaction, electrons were assumed to be transferred stepwise accompanied by proton removal. For example, one elementary step could be written in the form of reaction (1)

$$HA + h^+ + e^- \rightarrow A + H^+ + e^- \quad (1)$$

for which the Gibbs free-energy change is

$$\Delta G = G[A] + 0.5G[H_2] - G[HA] - G[h^+ + e^-] \quad (2)$$

where $G[h^+ + e^-]$ represents the free energy for the separation of an electron-hole pair.

$$G[H^+ + e^-] = e|U| = E_g + E_\gamma$$

where E_g is the band gap of the AgBr semiconductor and E_γ is the externally applied electrical energy at the onset potential for the water oxidation reaction. In a reported photoelectrochemical experiment,[35] the onset potential for the planar AgBr photoelectrode was 0.071 V (vs. NHE), and the band gap was estimated as 2.6 eV for all the systems. Therefore, e|U| in these systems should be 2.671 eV. In fact, the onset potential for AgBr(100) and (110) facets is different. However, compared with the value of the band gap, the difference is so small that it can be neglected. Thus, we use the same e|U| for different facets in our Gibbs free-energy calculations.

3. Results and discussion

3.1 Geometrical structures

The calculated lattice parameters of the clean AgBr crystal are given in Table 1, together with some other theoretical and experimental data for comparison. Our calculated crystal lattice constant is similar to the theoretical value reported in reference [36] (5.86 Å) and overestimates the experimental value (ca. 5.77 Å[13]) to some extent but is still closer to the experimental value than other theoretical results (6.057[37] and 5.9 Å[38]). The calculated cohesive energy of 5.10 eV is much closer to the experimental value (5.17 eV[39]) than another theoretical value (5.90 eV[40]). The calculated band gap (2.63 eV) is closer to the experimental value reported in reference [13] (2.6 eV) than the theoretical data reported previously (2.56[41] and 3.0 eV[42]). These fairly good agreements with experiments validate our theoretical approach to the geometrical and electronic structures of the systems studied.

Table 1. Calculated lattice constant a, cohesive energy E_{coh}, and band gap E_g of rock salt AgBr, compared to values from other experimental and theoretical works.

Parameters	Present work	Experimental	Other theoretical
a(Å)	5.865	5.77[13]	5.86,[36] 6.057,[37] 5.9[38]
E_{coh}(eV/cell)	5.10	5.17[39]	5.9[40]
E_g(eV)	2.63	2.6[13]	2.56,[41] 3.0[42]

As shown in Fig. 1a, different from the situation that both Ag and Br atoms are six coordinated in the bulk, a clean AgBr(100) facet has a nearly planar structure consisting of five-coordinate silver and bromine atoms. The square unit cell on the surface layer is alternatively encompassed by silver and bromine atoms with bond lengths of 2.944 Å, compared to the bulk length of 2.932 Å. The distance of the surface Ag/Br (Ag_{sur}/Br_{sur}) atom to the directly coordinated second layer bromine/silver (Br_{2c}/Ag_{2c}) is 2.849/2.969 Å (see Table 2), suggesting that the Ag_{sur} and Br_{sur} atoms are inward and outward relaxed with the respective values of -0.014 and 0.101 Å along the surface normal, due to the destruction of the lattice force field in the interface. The relaxation makes the surface layer be slightly undulated and thus establishes a surface electric double layer in the interface, which stabilizes the surface. The clean AgBr(110) facet, however, has a stepped structure with the alternative four-coordinate silver and bromine atoms along the [001] direction forming the edges of the steps, as shown in Fig. 1b. The V-type trough along the $[1\bar{1}0]$ direction is constructed alternatively by Ag-Br-Ag and Br-Ag-Br groups. This structural feature is commonly referred to as a saw-tooth profile. The distance of edge Ag (Ag_{ed}) and edge Br (Br_{ed}) is 2.953 Å, and the Ag_{ed} to the trough Br (Br_{tro}) distance is 2.778 Å while the Br_{ed} to the trough Ag (Ag_{tro}) distance is 2.850 Å (see Table 2), suggesting that both Ag_{ed} and Br_{ed} atoms exhibit relatively large outward relaxations, with values of 0.040 and 0.244 Å along the surface normal, while Ag_{tro} and Br_{tro} relax outward by 0.028 and 0.109 Å.

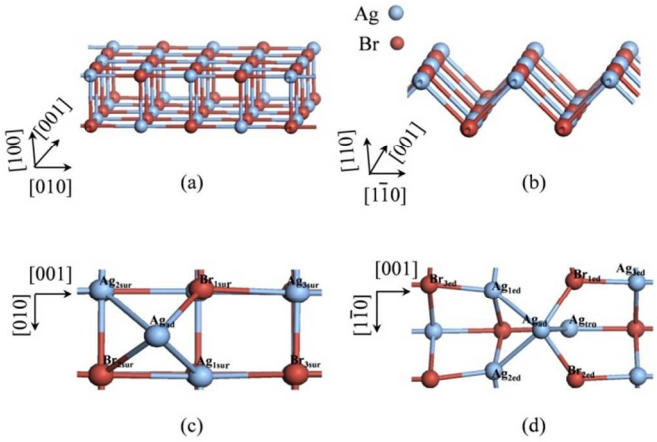

Fig. 1. Structures of the clean AgBr (100) (a) and (110) (b), adsorbed AgBr (100) (c), and (110) (d) facets.

All possible adsorption geometries of atomic Ag on the (110) and (100) facets of AgBr were checked. Although various sites can be visualized for the adsorption of Ag, only one stable structure was found on each surface. In the case of the adsorbed (100) facet, as shown in Fig. 1c, the adsorbed Ag (Ag_{ad}) is located at the four-fold hollow sites forming bonds with two adjacent Ag_{sur} and two adjacent Br_{sur} atoms at different distances (Ag_{ad}-Ag_{1sur}: 2.988 Å, Ag_{ad}-Ag_{2sur}: 3.014 Å, Ag_{ad}-Br_{1sur}: 2.953 Å, and Ag_{ad}-Br_{2sur}: 2.941 Å; Table 2). Owing to the interaction with Ag_{ad}, the relevant Ag_{sur} and Br_{sur} along the [010] direction (Ag_{1sur}-Br_{1sur} or Ag_{2sur}-Br_{2sur}) are pushed apart by 0.15 Å, and that along [001] direction (Ag_{1sur}-Br_{2sur} or Ag_{2sur}-Br_{1sur}) moves apart from 2.944 Å (on the clean facet) to 3.087 Å. The adsorption energy is calculated to be 0.46 eV.

For the adsorbed (110) facet, as shown in Fig. 1d, the Ag_{ad} atom bridges two adjacent stepped edges, tilted slightly towards a Br-Ag-Br V-type group, binding to all the atoms in the V group as well as adjacent Ag_{ed} atoms in the relevant edges. The distances of the newly-formed bonds are 2.695 (Ag_{ad}-Br_{1ed}), 2.699 (Ag_{ad}-Br_{2ed}), 3.144 (Ag_{ad}-Ag_{tro}), 2.902 (Ag_{ad}-Ag_{1ed}), and 2.891 Å (Ag_{ad}-Ag_{2ed}) (see Table 2). Due to the interaction with Ag_{ad}, the relevant Ag and Br atoms at the stepped edges are pushed apart by 0.69 and 0.72 Å for Ag_{1ed}-Br_{1ed} and Ag_{2ed}-Br_{2ed}, respectively, so that the bands are indeed ruptured. Correspondingly, the bonds of the relevant Ag and Br to the other adjacent Br_{ed} and Ag_{ed} atoms are shortened by 0.16 and 0.21 Å, and the distances to Br_{tro} and Ag_{tro} are enlarged by 0.06 and 0.17 Å. This system accounts for a relatively large adsorption energy of 1.42 eV, suggesting that atomic Ag tends to be adsorbed on the AgBr(110) facet.

Table 2. Ag-Br bond lengths (Å) for the clean and atomic Ag adsorbed (100) and (110) facets of AgBr.

Clean(100)[a]		Adsorbed(100)[a]		Clean(110)		Adsorbed(110)	
Ag_{sur}-Br_{sur}	2.944	Ag_{1sur}-Br_{2c}	2.926	Ag_{ed}-Br_{ed}	2.953	Br_{1ed}-Ag_{tro}	2.939
Ag_{sur}-Br_{2c}	2.849	Ag_{3sur}-Ag_{1sur}	2.893	Ag_{ed}-Br_{tro}	2.778	Ag_{1ed}-Br_{tro}	2.887
Br_{sur}-Ag_{2c}	2.969	Ag_{2sur}-Br_{1sur}	3.087	Br_{ed}-Ag_{tro}	2.850	Ag_{3ed}-Br_{1ed}	2.708
		Ag_{1sur}-Br_{1sur}	3.097			Ag_{1ed}-Br_{1ed}	3.650
		Ag_{1sur}-Ag_{3sur}	2.895			Ag_{1ed}-Br_{3ed}	2.730
		Ag_{1sur}-Br_{2sur}	3.087			Ag_{2ed}-Br_{2ed}	3.676
		Ag_{1sur}-Br_{2c}	2.852			Ag_{ad}-Br_{1ed}	2.695
		Ag_{ad}-Ag_{1sur}	2.988			Ag_{ad}-Ag_{1ed}	2.902
		Ag_{ad}-Br_{1sur}	2.953			Ag_{ad}-Br_{2ed}	2.699
		Ag_{ad}-Br_{2sur}	2.941			Ag_{ad}-Ag_{2ed}	2.891
		Ag_{ad}-Ag_{2sur}	3.014			Ag_{ad}-Ag_{tro}	3.144

[a] Ag_{2c} and Br_{2c} represent the directly bound atoms in the second layer.

The stability of facets can be closely related to the surface energy of the crystals, i.e., the smaller the surface energy, the higher the surface stability. The surface energy is calculated to be 0.172 J m^{-2} for the clean (110) facet and 0.035 J m^{-2} for the clean (100) facet, indicating that the clean (100) facet is much more stable than the clean (110) facet, in accordance with the theoretical results reported in references [21, 22]. Atomic silver adsorption substantially enhances the stability of both the (110) and (100) facets of AgBr, as mirrored by the decrease of the surface energies (0.093 and 0.019 J m^{-2}), but the adsorbed (100) facet is still more stable, even though it accounts for a much weaker adsorption of Ag.

3.2 Electronic structures

The total density of states (TDOSs) and partial density of states (PDOSs) for bulk AgBr are plotted in Fig. 2. The Fermi energy is set as the energy zero. The valence band (VB) shows dominant Ag 4d and Br 4p contributions included with minor Ag 5s and Ag 5p, and the dominant contribution near the valence band maxima (VBM) has the Br 4p character; while the conduction band (CB) comprises mainly Ag 5s and 5p states. It could be assumed that under appreciable photo-excitation electrons are mainly excited from the Br 4p orbitals to the Ag 5s/5p orbitals with photogenerated holes left behind in the Br 4p orbitals. It is this process that induces the photolysis of silver bromide and makes the instability of the material under sunlight.

Fig. 3 shows the TDOSs and PDOSs of clean AgBr(100) and AgBr(110) facets. The major contributions of the VB and CB are the same as those in the bulk AgBr. Although the two facets have almost the same VB and CB widths, the locations of the bands are different when going from one facet to the other, i.e., the (110) facet has a slightly higher VB in energy, whereas the CB is at slightly lower energy. Thus, the (110) facet is expected to have a narrower band gap and thus a shorter optical absorption threshold than the (100) facet. Moreover, the Br 4p density and thus the TDOS of the (110) facet are remarkably higher than those of (100) near VBM, thus the Br 4p states of the (110) facet is more profitable to be excited.

Interaction of Ag_{ad} with the facets is analyzed with PDOS plots, as shown in Fig. 4. Only the PDOS of each relevant atom in the energy range of interest is shown. The sum of the local DOS values of relevant Ag and Br atoms on the clean facets is also plotted for comparison. The energy zero of the plots corresponds to the Fermi level of the adsorbed AgBr system. Adsorption of Ag results in a remarkable change of the DOS feature of both facets, mirrored by the positions and structures of the bands. Especially, metal-induced gap states (MIGSs) are formed in the band gap of the clean facets. MIGSs have been reported for metal/semiconductor systems, e.g., Au adsorption on rutile TiO_2(110) surface, which are predominantly Au s-states;[41] adsorption of Pt_n (n=1-3) clusters on the defect-free anatase TiO_2(101) surface, which are predominantly Pt d-states although there are also small contributions from O states.[4]

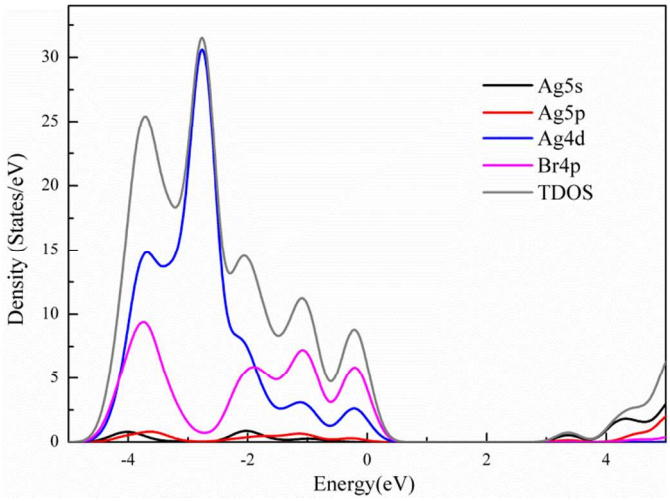

Fig. 2. Total density of states (TDOSs) and partial density of states (PDOSs) of Ag 5s, Ag 5p, Ag 4d, and Br 4p of bulk AgBr. The Fermi energy is set as the energy zero.

In the case of the adsorbed (110) facet (see Fig. 4a), the VB (from -6.8 to -1.4 eV) consists primarily of Ag_{ad} 4d, Ag_{ed} 4d, and Br_{ed} 4p states, and near VBM mainly of the Br_{ed} 4p character. In this band, mixing of Ag_{ad} 4d with Ag_{ed} 4d is the most strong and that with Br_{ed} 4p is considerable, but mixing of Br_{ed} 4p and Ag_{ed} 4d is relatively weak. The Ag_{ad}-Ag_{ed} and Ag_{ad}-Br_{ed} Mulliken overlap populations are calculated to be 0.52 and 0.21, but the Ag_{ed}-Br_{ed} overlap population cannot be calculated due to the large distance between them. These facts suggest that Ag_{ad} is indeed more strongly covalently bound to Ag_{ed} rather than to Br_{ed}, and the bond between Ag_{ed} and Br_{ed} is very weak due to the competition to form bonds with Ag_{ad}, in accordance with the adsorption structure as discussed above

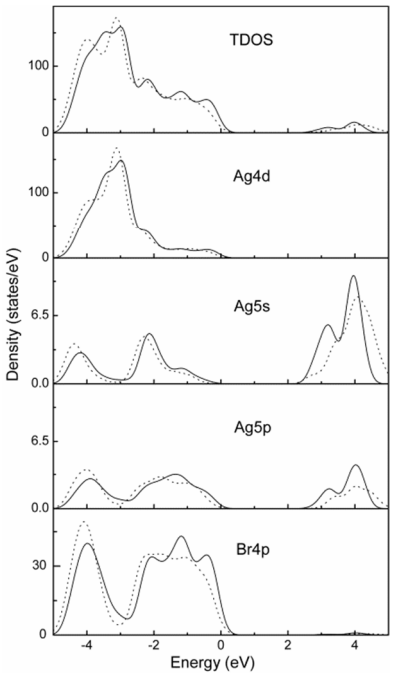

Fig. 3. Total density of states (TDOS) and partial density of states (PDOS) of Ag4d, Ag5s, Ag5p, and Br4p of the clean AgBr(110) (solid line) and the clean AgBr(100) (dot line) facets. The Fermi energy is set as the energy zero.

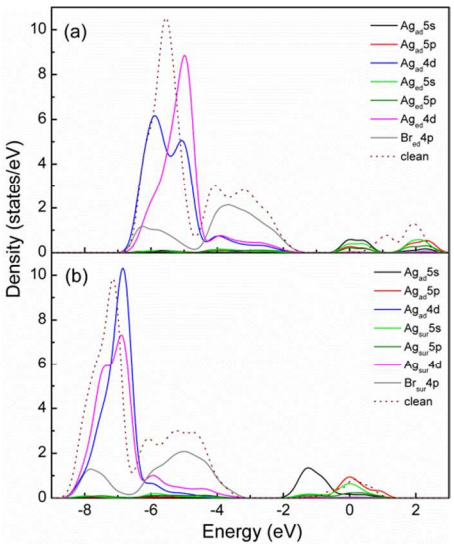

Fig. 4. Partial density of states (PDOSs) of Ag_{ad} 5s, 5p, relevant Ag_{ed} 5s, 5p, 4d, and Br_{ed} 4p of the adsorbed (110) facet (a); PDOSs of Ag_{ad} 5s, 5p, relevant Ag_{sur} 5s, 5p, 4d, and Br_{sur} 4p of the adsorbed (100) facet (b). The wine dot curve is the sum of local density of states (LDOSs) of Ag and Br atoms from the relaxed clean AgBr surface, and the energy is referred to the Fermi level of the Ag/AgBr system.

(see Fig. 1d). Because of the interaction of Ag_{ad}, the band corresponding to the clean facet CB splits into two bands, with a large band gap of 0.9 eV. The MIGS, the first one, located in the energy region from -0.5 to 0.9 eV is the result of bonding interaction of the 5s and 5p states of the Ag_{ad} and Ag_{ed} atoms, mirrored by the strong mixing of the states in the PDOS. The contributions of all these states are considerable. The importance decreases in the order of Ag_{ad} 5s, Ag_{ed} 5s, and comparable Ag_{ad} and Ag_{ed} 5p, contribution from Br_{ed} and Ag_{tro} and other states of Ag_{ad} and Ag_{ed} is negligible (see Fig. S1 in the ESI**)**. Since it is located just across the Fermi level, this band is expected to be partly occupied by electrons, resulting in metallization of the system. These findings are also supported by the Mulliken populations in the relevant orbitals (see Table S2 in the ESI). The second band (CB), from 1.4 to 2.9 eV, corresponds to the antibonding interaction of the relevant states, reflected by the strong mixing of the 5s and 5p states of Ag_{ad} and relevant surface Ag atoms, but in this case the relative contribution is different (Ag_{ad} 5p ≈ Ag_{ed} 5s > Ag_{ed} 5p > Ag_{ad} 5s). Also, this band is largely contributed by the Ag_{tro} 5s state, especially at the higher energy end **(**see Fig. S1 in the ESI). Obviously, the large gap between the bonding and antibonding bands suggests strong interaction of the relevant states, in agreement with the relatively strong interaction of Ag_{ad} with the surface as discussed in Section 3.1.

For the adsorbed (100) facet (see Fig. 4b), the VB (from -8.6 to -3.2 eV) also consists primarily of Ag_{ad} 4d, Ag_{sur} 4d, and Br_{sur} 4p states, and the Br_{sur} 4p character is also primary near VBM, but the extent of mixing between these components is different from the situation of the adsorbed (110) system, i.e., strong and considerable mixing are found for Ag_{sur} 4d with Ag_{ad} 4d and Br_{sur} 4p, and mixing between Br_{sur} 4p and Ag_{ad} 4d is very weak. The Mulliken overlap populations on Ag_{ad}-Ag_{sur}, Br_{sur}-Ag_{sur}, and Ag_{ad}-Br_{sur} are 0.41, 0.16, and -0.24, respectively. These facts suggest that Ag_{ad} is strongly covalently bound to Ag_{sur} but to Br_{sur} it is indeed an antibonding interaction, and the bond between the relevant Ag_{sur} and Br_{sur} is kept although it is a little weakened due to the competition to form bonds with Ag_{ad}, in accordance with the adsorption structure as discussed above (see Fig. 1c). The band corresponding to the original CB of the clean facet shows also somewhat splitting as a result of interaction with Ag_{ad}, but to a less extent, as compared to that of the adsorbed (110), so that the splitted bands overlap in the range of -0.7 to -0.3 eV. The lower-energy band (the MIGS) in the energy region from -2.0 to -0.3 eV is the bonding state, consisting predominantly of the Ag_{ad} 5s state with very minor Ag_{sur} 5s/5p and Ag_{ad} 5p, contributions from Br_{sur} atoms and other states of both Ag_{ad} and Ag_{sur} are negligible. This band is expected to be fully occupied. The higher-energy band (CB) is present in the region of -0.7 to 1.5 eV, constructed also by strong mixing of the 5s and 5p states of Ag_{ad} and the relevant Ag_{sur} atoms (antibonding interaction), with the relative contribution following Ag_{ad} 5p > Ag_{sur} 5s > Ag_{sur} 5p > Ag_{ad} 5s. This band is expected to be partly occupied by electrons, supported by the Mulliken population of the relevant orbitals listed in Table S2 in the ESI. Obviously, the relatively small splitting of the bonding and antibonding bands indicates that the interaction of Ag_{ad} with Ag_{sur} is not as strong as that in the adsorbed (110) system, in accordance with the adsorption energies as given in Section 3.1.

We also calculated the band structure of the bulk AgBr (see Fig. S2 in the ESI), clean and adsorbed (110) and (100) facets (see Fig. 5). The band structure of the bulk AgBr reveals a direct band gap of 3.97 eV and an indirect band gap of 2.63 eV between VB and CB, agreeing well with the experimental values.[17] The band gaps of the clean (100) and (110) facets are 2.35 and 2.15 eV, smaller than the value of bulk AgBr (2.63

eV) due mainly to the surface relaxation and reconstruction. As shown in Fig. 5b,c, compared with the clean (110) facet, adsorption of Ag results in movement of both the VB and CB of the adsorbed (110) facet to lower energies, and the relatively large VB movement enlarges the intrinsic band gap (cal. 2.3 eV). In addition, the metal-induced gap band (MIGB) of the adsorbed (110) facet is formed in the energy region from -0.2 to 0.5 eV (α and β states are shown in the Figure) due to the adsorption of Ag. The VB to MIGB gap is narrower than the intrinsic band gap (1.5 vs. 2.15 eV), it is thus conducive to the redshift of the photoabsorption spectroscopy. The MIGB is expected to be partly occupied because it crosses the Fermi level, in accordance with the PDOS in Fig. 4.

In the case of the adsorbed (100) facet (Fig. 5e,f), both the VB and CB are also moved to lower energies, but to larger extents than those for the adsorbed (110) facet. A number of the CB energy levels corresponding to the clean (100) facet is moved to positions across the Fermi level, which are expected to be partly occupied, causing metallization of the system. Furthermore, the relatively large VB movement enlarges the intrinsic band gap (cal. 2.6 eV), and the MIGB is below the Fermi level, it is thus expected to be fully occupied. The distance of MIGB to CB is very small (< 1.7 eV), which is conducive to the electronic transitions upon the absorption of visible and infrared light.

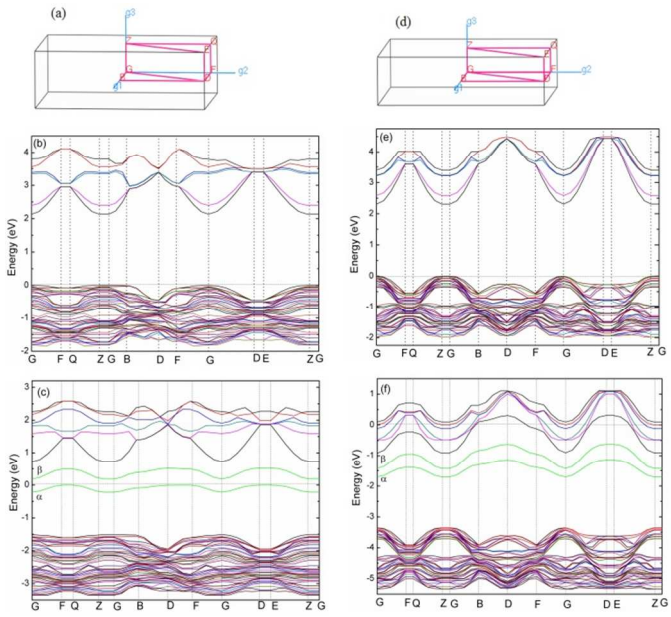

Fig. 5. Brillouin zone of AgBr(110) facet (a), band structure of the clean (b) and adsorbed (c) AgBr(110) facets; Brillouin zone of AgBr(100) facet (d), band structure of the clean (e) and adsorbed (f) AgBr(100) facets.

From the curvatures of the bands of the clean (100) and (110) facets, the electron effective masses are estimated to be approximately 0.20 and 0.15 m_0, while the hole-effective masses are estimated to be approximately 1.01 and 0.46 m_0, respectively. The calculated electron and hole effective masses are similar to those of the rock-salt phase reported in reference [44] (0.230 and 1.019 m_0). Since the drift velocity of electrons or holes is proportional to the reciprocal of the effective mass, lower effective masses imply more efficient charge-carrier transport.[32] Thus, the clean (110) facet with lower electron and hole effective masses has a higher drift velocity of photogenerated electrons and holes than the clean (100) facet.

The electron effective masses on the adsorbed (100) and (110) facets are estimated to be approximately 0.15 and 0.12 m_0 (using the lowest band above the Fermi level), respectively. Both of them are smaller than those of the clean facets. Thus, electrons on the adsorbed facets have more possibility of transport than on the clean facets, which would be conducive to reactions on the facets. This feature would be further proved in water dissociation.

3.3 Optical properties

Fig. 6 presents the calculated absorption coefficients of the clean and adsorbed (100) and (110) facets. Although the maximum absorption coefficient changes slightly, the absorption threshold for the clean surface along the [110] direction is near 450 nm, approximately 50 nm longer than that along the [100] direction, in agreement with the feature of the DOSs and band structures shown in Figures 3 and 5. The calculated absorption spectra are also in good agreement with the experimental spectra reported in references [13, 45].

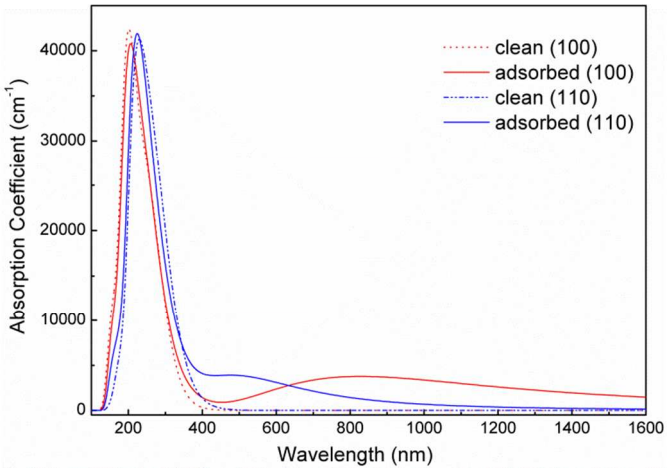

Fig. 6. The calculated absorption coefficients of the clean and adsorbed (100) and (110) facets of AgBr.

Compared with the clean facets, strength, threshold, and region of the fundamental absorption of the adsorbed systems change slightly, while the spectral response range is largely widened to the visible and even the infrared regions, and the absorption coefficient shows features with a low shoulder at 500 nm for the adsorbed (110) facet and a peak at 800 nm for the adsorbed (100) facet. Interestingly, although the absorption coefficient of the adsorbed (100) facet is higher than that of the adsorbed (110) facet in the longer wavelength (mainly the infrared) region, the adsorbed (110) facet shows stronger absorption coefficients in the visible region, which is just the main part of the solar irradiation (~50%). Thus, it is expected that Ag adsorption on AgBr(110) can efficiently enhance the quantum yields and the visible light utilization of the photocatalyst.

As discussed above, the band structures relevant to the absorption spectra can be simplified as VB+MIGB+CB. Based on the DOS features (Fig. 4) and the band structures (Fig. 5), the fundamental absorption in the absorption spectrum of the adsorbed (100) facet arises from the electronic excitation from VBM to CB (above the Fermi level), attributed to the photo-excitation of Br 4p to the antibonding states of Ag_{ad} 5p and

Ag_{sur} 5s states. The larger contribution of the Ag_{ad} 5p state than the Ag_{sur} 5s state in the CB reduces the intrinsic transition of photo-excitation electrons (Br4p → Ag5s) and enhances the stability of silver bromide.

We can also identify the absorption in wavelengths longer than 600 nm arising from transitions from MIGB and CB (below the Fermi level) to CB (above the Fermi level), which is mainly the photo-excitation from Ag_{ad} 5s to Ag_{ad} 5p and Ag_{sur} 5s/5p antibonding states. Note that in this case electron transfers from Br to the adsorbed and relevant surface Ag atoms are not involved. On the other hand, the fundamental absorption in the absorption spectrum of the adsorbed (110) facet arises from the electronic transition from VBM to CBM, attributed to the photo-excitation of Br 4p to the 5s and 5p hybridized antibonding state of Ag_{ad} and Ag_{ed}, and the absorption appearing in 450 - 800 nm is attributed to the VBM to MIGB (above the Fermi level) transition, which is the excitation from Br 4p to Ag_{ad} 5s/5p and Ag_{ed} 5s/5p bonding state, as well as the MIGB (near the Fermi level) to CB transition. We can find that the photo-excitation in the whole absorption spectrum of the adsorbed (110) facet involves dominantly electron transfers from Br to the adsorbed and relevant surface Ag atoms, facilitating reduction of organic species occurring on these metal atoms as well as oxidation reactions on Br atoms and enhancing the stability of silver bromide. Thus, the adsorbed AgBr(110) facet should possess better photocatalytic performance than the adsorbed AgBr(100) facet.

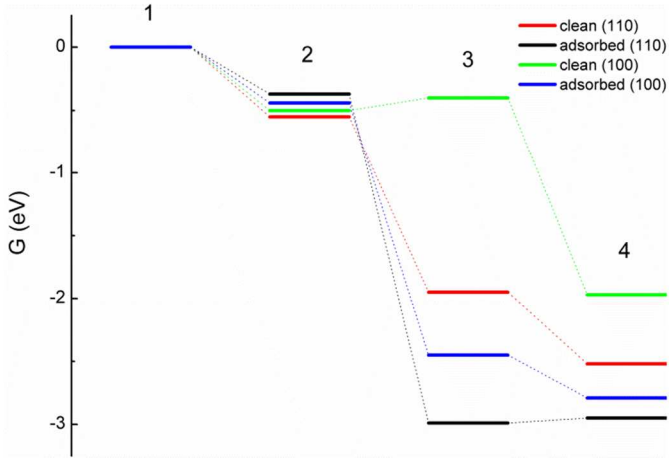

Fig. 7. Free-energy profiles of water dissociation on the clean and adsorbed (100) and (110) facets of AgBr with e|U|=2.671 eV. **1**: AgBr, **2**: H_2O*-AgBr, **3**: HO*-AgBr, and **4**: O*-AgBr (see Fig. S3 in the ESI).

3.4 Water dissociation on AgBr surfaces

Although the photocatalytic activity of silver/silver halides is experimentally evaluated by photodegradation of methyl orange dye and rhodamine-B under visible-light irradiation,[20-22] the Ag/AgBr nanocomposites also show excellent photocatalytic activity for conversion of CO_2 with H_2O to energetic fuels, e.g., methanol/ethanol, under visible light irradiation, in which hydrogen ions are produced by water oxidation with the help of the photogenerated holes over the catalysts.[19] Indeed, the possibility of the photocatalytic water dissociation on AgBr producing O_2 can be evaluated by the VBM position of the bulk AgBr (-0.79 eV vs NHE; see Section S1 in the ESI), compared to the potential of $\psi^0(O_2/H_2O) = -1.23\ eV$ (vs NHE), and the CBM position of the bulk AgBr (-3.42 eV vs NHE), lower than $\psi^0(H_2/H_2O) = 0\ eV$ (see Section S1 in the ESI), implies that the photocatalysis of water on AgBr can only produce H^+, which may take part in other complex photoinduced reactions. Furthermore, the sunlight-driven water dissociation is an attractive approach to utilize solar energy, and its photocatalytic mechanism is well understood.[46] For these reasons, water dissociation is chosen as a probe reaction to explore the catalytic activity of the clean and adsorbed AgBr facets. On the basis of the reported intermediates and local surface structures,[34] the most possible channel of water dissociation is tested, in which the structure with the lowest energy is recognized as the intermediate of each step. The lowest-energy pathways on the clean and adsorbed (110) and (100) facets are shown in Fig. 7, and the corresponding intermediate structures in Fig. S3 in the ESI.

On the clean (100) facet, the O atom of water sits on top of an Ag_{sur} with a distance of 2.479 Å and a 8.5° angle of O-Ag_{sur} to the surface normal, the H atoms point into the vacuum with O-H bond lengths of 0.948 Å and a H-O-H angle of 104.4°(see Fig. S3c in the ESI), quite similar to the gas-phase structure. The adsorption energy is calculated to be 0.5 eV. When the first proton is removed, the O atom of OH is still located above the Ag_{sur} due perhaps to the geometrical effect as well as the highest stability of the (100) facet as discussed in Section 3.1. The angle of H-O-Ag_{sur} is enlarged 10.6° than that of the adsorbed H_2O. This structure accounts for the highest location in energy of the intermediate among all the four analogues, causing the free-energy profile go uphill by 0.1 eV. While the free-energy profile goes downhill by 1.57 eV followed the second proton removed, and the O adatom is also adsorbed at the top of the Ag_{sur} atom (1.909 Å) and it locates still the highest in energy among the four cases as shown in Fig. 7.

On the clean (110) facet, the adsorption energy of H_2O (0.55 eV) is larger than that on the clean (100) facet. In this case, the O atom of water sits atop an Ag_{ed} at a distance of 2.331 Å, tilted by 15.6° to the surface normal (see Fig. S3a in the ESI), the O-H bond lengths are 0.947 and 0.959 Å and the H-O-H angle is 106.5°. When the first proton is removed, the free-energy profile drops by 1.4 eV, instead of going uphill as in the analogous step on the clean (100) facet, indicating that the clean (110) facet favors the initial step of water dissociation. The large stabilization of the intermediate is caused by the fact that the newly-formed OH moiety immediately bonds to two Ag_{ed} cations from adjacent edges via the O atom, forming a bridge site adsorption configuration. As the reaction continues, the free-energy profile goes downhill by 0.57 eV, much smaller than that on the clean (100) facet. The resulting O adatom bonds also to adjacent Ag cations at the distance of 1.965 Å. The bond is so strong that direct release of O is energetically impossible. Thus, the total energy drop after the first and second proton removals on the clean (110) facet (1.97 eV) is larger than that on the clean (100) facet (1.47 eV). Therefore, dissociation of H_2O will take place more readily on the clean (110) facet.

On the adsorbed (100) facet, adsorption of H_2O is also through its O at the Ag_{ad} with the distance of 2.376 Å, the adsorption energy is 0.44 eV. Both the first and second proton removals result in drops of energy (by 2.01 and 0.35 eV). The OH moiety and O adatom bond to Ag_{ad} at distances of 1.933 and 1.900 Å. The total energy profile drops by 2.36 eV after the first and second proton removals, compared to the 1.47 eV drop in the analogous processes on the clean (100) facet. Moreover, the reaction occurs more possibly near the Ag_{ad}. Thus, adsorption of Ag on (100) could also facilitate dissociation of H_2O remarkably.

The adsorption energy of H_2O on the adsorbed (110) facet is calculated to be 0.37 eV. In this case, the O atom of water prefers the Ag_{ad} at 2.401 Å, both O-H bond lengths are 0.948 Å and the bond angle is 105.3°. When the first proton is removed, the free-energy profile drops by 2.62 eV, larger than that of the analogous step on the clean (110) facet (1.4 eV). The OH moiety bonds directly to Ag_{ad} and two Ag_{ed} cations via O atom at different distances (cal. 2.180, 2.262, and 2.274 Å). When the second proton is removed, the free-energy profile goes uphill by 0.04 eV. The O adatom also bonds to the Ag_{ad} and two relevant Ag_{ed} cations with bond lengths of 1.979, 2.123, and 2.126 Å. Since both the first and second proton removals of H_2O occur on Ag_{ad} and its relevant Ag_{ed} atoms, we can conclude that photoinduced electron aggregating on Ag_{ad} and relevant Ag_{ed} would facilitate the reaction. The overall drop of energy (2.58 eV) after the first and second proton removals on the adsorbed (110) facet is larger than the values of the analogous processes on both the clean (110) facet (1.97 eV) and the adsorbed (100) facet (2.36 eV). Therefore, the adsorbed (110) facet favors the photoinduced dissociation of H_2O than either the clean (110) or the clean and adsorbed (100) facets, and may show the highest photocatalytic activity among all the four facets studied.

4. Conclusions

In this article, we have systematically investigated the photocatalytic properties of the clean and atomic Ag adsorbed (100) and (110) surfaces of AgBr using DFT plus Hubbard U contributions. Compared with the clean (100) surface, the clean (110) surface has a lower surface stability and a narrower band gap. Both the clean surfaces have strong absorption coefficiencies in the UV region, arising mainly from the electronic transition of Br 4p to Ag 5s/5p, and the absorption threshold of the (110) facet (450 nm) is about 50 nm longer than that of (100).

Atom Ag_{ad} prefers to bind to all atoms in a V-type Br-Ag-Br group and two neighbor Ag atoms from adjacent edges on the saw-tooth (110) facet, while on (100) it is adsorbed to two surface Ag's and two surface Br's. The relatively strong adsorption of Ag on (110) largely splits the clean surface CB into two bands (MIGS and CB), while on (100) the splitting is relatively small. The Ag_{ad} wave functions mix with the orbitals of the silver ions of the silver bromide，which obviously impact on the electron states of the conduction band bottom. Compared with the clean facets, the adsorbed (110) surface favors a new visible absorption with a shoulder at 500 nm, involving dominantly electron transfers from Br to the hybridized orbitals, while an infrared absorption (> 600 nm) is largely enhanced for the adsorbed (100), attributed to excitation of states of Ag_{ad} and the hybridized orbitals. Therefore, the Ag_{ad} atom as well as the surface play an important role in the visible light absorption. The overall free-energy drop of water dissociation follows the order Ag/AgBr(110) > Ag/AgBr(100) > AgBr(110) > AgBr(100), suggesting that Ag/AgBr(110) indeed has the highest catalytic activity.

The present work not only explains reasonably the experimental phenomena, but also serves as a starting point for our future study of Ag_n/AgBr and Ag_n/AgBr/X (X denotes support materials) photocatalyts.

Acknowledgements

This work was supported by the Program for NSFC (21003158 and 21303266), Shandong Province Natural Science Foundation (ZR2011EMZ002), Taishan Scholar Foundation (ts20130929), Promotive Research Fund for Excellent Young and Middle-aged Scientists of Shandong Province (BS2012NJ015), and the Fundamental Research Funds for the Central Universities (12CX02014A, 14CX02004A, 14CX06001A, 13CX02001A and 13CX05020A).

Notes and references

[a] *College of Science, China University of Petroleum, Qingdao, Shandong 266580, P. R. China*
[b] *Key Laboratory of New Energy Physics & Materials Science in Universities of Shandong Province, China University of Petroleum, Qingdao, Shandong 266580, P. R. China*
[c] *State Key Laboratory of Heavy Oil Processing, Key Laboratory of Catalysis, CNPC, China University of Petroleum, Qingdao 266580, P. R. China*
[d] *Department of Physics and Materials Science, City University of Hong Kong, Hong Kong SAR, P. R. China*
E-mail: wyguo@upc.edu.cn (W. Guo); liuyq@upc.edu.cn (Y. Liu).

† Electronic Supplementary Information (ESI) available: Details of the U parameters, the calculated Mulliken atomic populations, some PDOS of Ag adsorbed (110) facet, band structure of bulk, intermediated structures for water dissociation, and estimation of the positions of the conduction band and the valence band. See DOI: 10.1039/b000000x/

1 G. Liu, J.C. Yu, G.Q. Lu and H. M. Cheng, *Chem. Commun.* **2011**, *46*, 6763.
2 H. Yang, C Sun, S. Qiao, J. Zou, G. Liu, S. H. Cheng and G. Q. Lu, *Nature* **2008**, *453*, 638.
3 B. T. Qiao, A. Q. Wang, X. F. Yang, L. F. Allard, Z. Jiang, Y. T. Cui, J. Y. Liu, J. Li and T. Zhang, *Chem.* **2011**, *3*, 634.
4 Y. Han, C. Liu and Q. Ge, *J. Phys. Chem. B* **2006**, *110*, 7463.
5 H. Tong, S.X. Ouyang, Y. P. Bi, N. Umezawa, M. Oshikiri and J. H. Ye, *Adv. Mater.* **2012**, *24*, 229.
6 G. Liu, C. H. Sun, H. G. Yang, S. C. Smith, L. Z. Wang, G. Q. Lu and H. M. Cheng, *Chem. Commun.* **2010**, *46*, 755.
7 S. Hong and T. S. Rahman, *J. Am. Chem. Soc*. **2013**, 135, 7629.
8 H. G. Yang, G. Liu, S. Z. Qiao, C. H. Sun, Y. G. Jin, S. C. Smith, J. Zou, H. M. Cheng and G. Q. Lu, *J. Am. Chem. Soc.* **2009,** *131,* 4078.
9 A. S. Barnard and L. A. Curtiss, *Nano Lett.* **2005**, *5*, 1261.
10 X. Q. Gong, A. Selloni, M. Batzill and U. Diebold, *Nat. Mater.* 2006, *5*, 665.
11 J. A. Rodríguez, J. Evans, J. Graciani, J.-B. Park, P. Liu, J. Hrbek and J. F. Sanz, *J. Phys. Chem. C* 2009, *113*, 7364.
12 K. Awazu, M. Fujimaki, C. Rockstuhl, J. Tominaga, H. Murakami, Y. Ohki, N. Yoshida and T. Watanabe, *J. Am. Chem. Soc.* 2008, *130*, 1676.
13 P. Wang, B. B. Huang, X. Y. Qin, X. Y. Zhang, Y. Dai, Z. Wang and Z. Lou, *ChemCatChem* **2011**, *3*, 360.
14 Y. P. Bi and J. H. Ye, *Chem. Eur. J.* **2010**, *16*, 10327.
15 G. Li, K. H. Wong, X. Zhang, C. Hu, J. C. Yu, R. C. Y. Chan and P. K. Wong, *Chemosphere* **2009**, *76,* 1185.
16 R. Dong, B. Tian, C. Zeng, T. Li, T. Wang and J. Zhang, *J. Phys. Chem. C* **2013**, 117, 213.
17 S. Glaus, G. Calzaferri and R. Hoffmann, *Chem. Eur. J.* **2002**, 8, 1785.
18 N. Kakuta, N. Goto, H. Ohwaki and T. Mizushima, *J. Phys. Chem. B* **1999**, *103*, 5917.
19 C. An, J. Wang, W. Jiang, M. Zhang, X. Ming, S. Wang and Q. Zhang, *Nanoscale* 2012, *4*, 5646.
20 L. Kuai, B. Geng, X. Chen, Y. Zhao and Y. Luo, *Langmuir* **2010**, *26*, 18723.
21 H. Wang, J. Yang, X. Li, H. Zhang, J. Li and L. Guo, *Small* **2012**, *8*, 1.

22 H. Wang, X. Lang, J. Gao, W. Liu, D. Wu, Y. Wu, L. Guo and J. Li, *Chem. Eur. J.* **2012**, *18*, 4620.
23 X. Zhou, C. Hu, X. Hu, T. Peng and J. Qu, *J. Phys. Chem. C* **2010**, 114, 2746.
24 X. Wang, Y. Tang, Z. Chen and T.-T. Lim, *J. Mater. Chem.* **2012**, 22, 23149.
25 R. C. Baetzold, *J. Phys. Chem. B* **2001**, *105*, 3577.
26 R. C. Baetzold, *J. Phys. Chem. C* **2007**, 111, 1385.
27 F. Rabilloud, F. Spiegelman, J. M. L'Hermite and P. Labastie, *J. Chem. Phys.* **2001**, *114*, 289.
28 P. Gutta and R. Hoffmann, *J. Phys. Chem. A* **2003**, 107, 8184.
29 L. Thulin and J. Guerra, *Phys. Rev. B* **2008**, *77*, 195112.
30 N. N. Lathiotakis, A. N. Andriotis and M. Menon, *Phys. Rev. B* **2008**, *78*, 193311.
31 W. Kohn and L. Sham, *J. Phys. Rev. B* **1965**, *140*, A1133.
32 J. P. Perdew, K. Burke and M. Ernzerhof, *Phys. Rev. Lett.* **1996**, *77*, 3865.
33 R. M. Sheetz, I. Ponomareva, E. Richteret, A. N. Andriotis and M. Menon, *Phys. Rev. B* **2009**, *80*, 195314.
34 J. Yang, D. Wang, X. Zhou and C. Li, *Chem. Eur. J.* **2013**, *19*, 1320.
35 P. Yin, W. Hou, L. Xu, J. Wang and Y. Xin, *Corros. Sci. Pro. Tech.* **2010**, *22*, 407.
36 L. A. Palomino-Rojas, M. López-Fuentes, G. H. Cocoletzi, G. Murrieta, R. D. Coss and N. Takeuchi, *Solid State Sci.* **2008**, *10*, 1228.
37 T. Söhnel, H. Hermann and P. Schwerdtfeger, *J. Phys. Chem. B* **2005**, *109*, 526.
38 Y. Li, L. Zhang, T. Cui, Y. Ma, G. Zou and D. D. Klug, *Phys. Rev. B* **2006**, *74,* 054102.
39 R. K. Singh and P. Khare, *Phys. Stat. Sol. (B)* **1981**, *103*, 337.
40 G. S. Nunes and P. B. Allen, *Phys. Rev. B* **1998**, *57*, 5098.
41 C. M. I. Okoye, *Solid State Commun.* **2004**, *129*, 69.
42 R. H. Victora, *Phys. Rev. B* **1997**, *56*, 4417.
43 N. Lopez and J. K. Nørskov, *Surf. Sci.* **2001**, *515*, 175.
44 T. Benmessabih, B. Amrani, F. E. H. Hassan, F. Hamdache and M. Zoaeter, *Phys. B* **2007**, *392*, 309.
45 L. Nie, Z. Huang, H. Xu, W. Zhang, B. Yang, L. Fang and S. Li, *Chin. J. Catal.* **2012**, *33*, 1209.
46 S. Y. Reece, J. A. Hamel, K. Sung, T. D. Jarvi, A. J. Esswein, J. J. H. Pijpers and D. G. Nocera, *Science* **2011**, *334*, 645.